

# CO<sub>2</sub> dissolution in a background hydrological flow

H. Juliette T. Unwin\*

Garth N. Wells†

Andrew W. Woods‡

## Abstract

During CO<sub>2</sub> sequestration into a deep saline aquifer of finite vertical extent, CO<sub>2</sub> will tend to accumulate in structural highs such as offered by an anticline. Over times of tens to thousands of years, some of the CO<sub>2</sub> will dissolve into the underlying groundwater to produce a region of relatively dense, saturated water directly below the plume of CO<sub>2</sub>. Continued dissolution then requires the supply of unsaturated aquifer water. In an aquifer of finite vertical extent, this may be provided by a background hydrological flow, or a laterally-spreading buoyancy-driven flow caused by the greater density of the CO<sub>2</sub> saturated water relative to the original aquifer water.

We investigate the long time steady-state dissolution in the presence of a background hydrological flow. In steady-state, the distribution of CO<sub>2</sub> in the groundwater upstream of the aquifer involves a balance between three competing effects: (i) the buoyancy-driven flow of CO<sub>2</sub> saturated water; (ii) the diffusion of CO<sub>2</sub> from saturated to under-saturated water; and (iii) the advection associated with the oncoming background flow. This leads to three limiting regimes. In the limit of very slow diffusion, a nearly static intrusion of dense fluid may extend a finite distance upstream, balanced by the pressure gradient associated with the oncoming background flow. In the limit of fast diffusion relative to the flow, a gradient zone may become established in which the along aquifer diffusive flux balances the advection associated with the background flow. However, if the buoyancy-driven flow speed exceeds the background hydrological flow speed, then a third, intermediate regime may become established. In this regime, a convective recirculation develops upstream of the anticline involving the vertical diffusion of CO<sub>2</sub> from an upstream propagating flow of dense CO<sub>2</sub> saturated water into the downstream propagating flow of CO<sub>2</sub> unsaturated water. For each limiting case, we find analytical solutions for the distribution of CO<sub>2</sub> upstream of the anticline, and test our analysis with full numerical simulations. A key result is that, although there may be very different controls on the distribution and extent of CO<sub>2</sub> bearing water upstream of the anticline, in each case the dissolution rate is given by the product of the background volume flux and the difference in concentration between the CO<sub>2</sub> saturated water and the original aquifer water upstream.

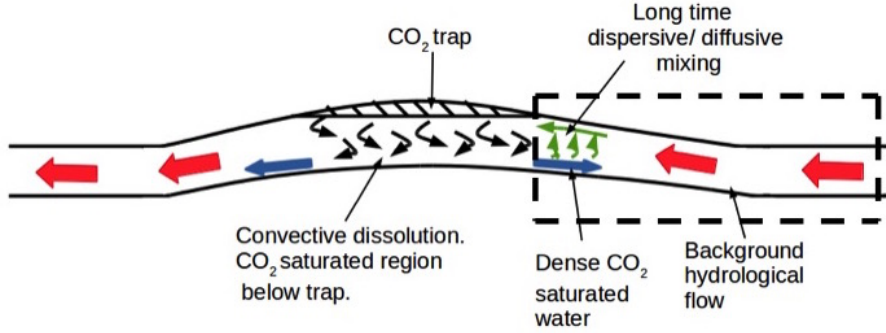
## 1 Introduction

Carbon capture and storage in deep saline aquifers has been proposed as a potential means to limit carbon emissions into the atmosphere, while enabling the continued supply of energy from fossil fuels. Much research has been undertaken to explore the processes which control the storage of CO<sub>2</sub> over very long periods, and in particular the integrity of a geological storage facility in terms of the possible migration of CO<sub>2</sub> back to the surface [2, 3, 10, 15]. Owing to the buoyancy of CO<sub>2</sub> relative to water at depths of 1–2 km, CO<sub>2</sub> tends to migrate along permeable sedimentary layers and ultimately ponds in structural highs, for example an anticline, which represents the upper part of a fold or other deformation in the geological strata (see Figure 1a). Such structural traps offer a possible storage site providing there is a competent seal rock above the anticline (e.g., IPCC 6). However, CO<sub>2</sub> is soluble in groundwater, which may accommodate concentrations

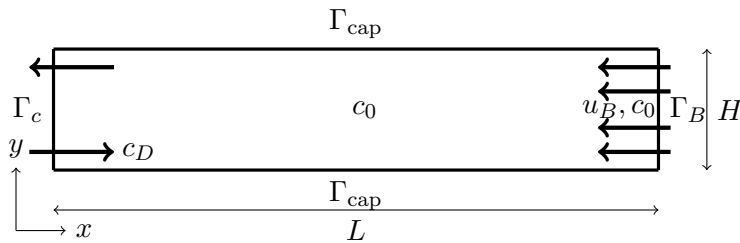
\*Department of Engineering, University of Cambridge (hjt2@cam.ac.uk)

†Department of Engineering, University of Cambridge (gnw20@cam.ac.uk)

‡BP Institute, University of Cambridge (andy@bpi.cam.ac.uk)



(a) Cartoon of the geological problem with region of interest indicated by dashed box. The large red arrows represent the direction of the background hydrological flow, while the smaller black curved arrows below the CO<sub>2</sub>, which is trapped at the top of the anticline, represent the convective mixing of the CO<sub>2</sub> saturated and undersaturated water. The smaller blue arrow inside the dashed box represents the buoyancy driven flow of dense CO<sub>2</sub> saturated water flowing upstream into the background hydrological flow.



(b) Model problem for analysis and simulation.

Figure 1: Problem of interest.

of a few wt% CO<sub>2</sub> in solution. This in turn leads to an increase in density of the water. With the dependency of water density on CO<sub>2</sub> concentration, convectively-driven dissolution may develop. Water below the trapped CO<sub>2</sub> plume becomes increasingly concentrated in CO<sub>2</sub> until it becomes convectively unstable and sinks into the underlying permeable rock, to be replaced by less dense, unsaturated water (c.f. Hewitt et al. 4, Lindeberg and Wessel-Berg 7, Pau et al. 9, Riaz et al. 11). Eventually, the water below the CO<sub>2</sub> plume becomes fully saturated and the continued dissolution requires a more distal supply of undersaturated groundwater.

Szulczewski et al. [12] examined the longer-time dissolution by examining the convective exchange flow which can develop in a horizontal aquifer. They established that following the initial dissolution and near-saturation of the groundwater directly below the plume of CO<sub>2</sub>, the lateral convective exchange flow leads to the slow horizontal spreading of a zone of CO<sub>2</sub> enriched groundwater associated with the continued dissolution. Eventually, the dynamics of this zone may become controlled by a balance between: (a) the buoyancy-driven shear, as the dense groundwater spreads along the base of the aquifer; and (b) the vertical diffusion of CO<sub>2</sub> from this outward spreading dense fluid to the return flow of under-saturated groundwater higher in the aquifer. By itself, such buoyancy-driven shear dispersion leads to a progressively waning rate of dissolution, and, owing to the relatively low solubility of CO<sub>2</sub> in the ground water, the prediction that the plume of CO<sub>2</sub> may be trapped in the anticline for a very long time [12].

However, at long times the slow background hydrological flows which transport fluid laterally through aquifers will become important in controlling the flux of unsaturated water from far upstream, especially as other transport processes wane. It is the purpose of this paper to explore the long term influence of a background hydrological flow on the process. In this context,

Woods and Espie [17] established some non-linear bounds on the flux of groundwater that may reach an anticline along a weakly tilted aquifer resulting from the interaction of a background hydrological flow with a convective exchange flow for intermediate times, during which the cross-aquifer diffusive transport of  $\text{CO}_2$  is small. In the present work, we account for the effects of such diffusion and this leads to a more complex problem involving the interaction of the background advection, the buoyancy-driven flow and the diffusive transport of  $\text{CO}_2$  upstream of the anticline. We note that in our modelling we assume the background hydrological flows are constant in time and that there are no mineralogical reactions of the  $\text{CO}_2$  with the formation; these are simplifications but provide a reference with which the effects of mineral precipitation or changes in the background forcing over time could be compared.

We develop a series of idealised, analytical solutions for the governing equations and then test these solutions using a full numerical simulation of the two-dimensional governing equations. In modelling the flow in porous rock, we assume that the dynamics are governed by Darcy's Law, which relates to slow viscous flow. This is an appropriate model in the present content of slow hydrological flows and the slow buoyancy driven flow of  $\text{CO}_2$  saturated water (e.g. Bear 1, Woods 16). We thereby establish that when the buoyancy-driven flow of the dense  $\text{CO}_2$  saturated water is large compared to the background flow speed, which is typical, three different regimes may become established: (i) the weak diffusion limit in which there is a nearly static intrusion of  $\text{CO}_2$  saturated water upstream; (ii) an intermediate regime in which there is a balance of buoyancy-driven flow and vertical diffusion with the oncoming flow; and (iii) a strong diffusion limit, in which there is a balance between the upstream diffusion of  $\text{CO}_2$  and the downstream advective transport of unsaturated water. In each case, the dissolution rate is proportional to the groundwater flow, even though the controls on the extent of the  $\text{CO}_2$  enrichment of the groundwater upstream of the anticline may be very different.

## 2 Model system

In our analysis, we consider a two-dimensional flow geometry, shown in Figure 1. This corresponds to an anticline produced by a fold in the geological strata that extends for a relatively long distance in the direction normal to the page compared to the width of the fold. We consider a background hydrological flow that supplies fluid from the right-hand side, and an aquifer that is of uniform thickness and horizontal. We assume that directly below the plume of  $\text{CO}_2$  which is trapped in the anticline, the water is fully saturated in  $\text{CO}_2$  as a result of the vertical convective dissolution, and that this is carried downstream (to the left in Figure 1a). The primary purpose of this paper is to examine how the concentration of  $\text{CO}_2$  varies in the upstream direction, shown in Figure 1b. In our numerical model, we choose the location of the upstream boundary of the flow domain to be upstream of the region containing elevated concentrations of  $\text{CO}_2$ , so that we can impose a simple uniform flow of fluid with uniform background  $\text{CO}_2$  concentration.

The full model involves Darcy flow with a buoyancy term that is dependent on the dissolved  $\text{CO}_2$  concentration  $c \in [c_0, c_D]$ , where  $c_0 \geq 0$  is the initial  $\text{CO}_2$  mass fraction of the groundwater and  $c_D$  is the mass fraction of the  $\text{CO}_2$  saturated groundwater below the trapped plume of  $\text{CO}_2$  (see Figure 1b). We assume a fluid density  $\rho$  given by

$$\rho = \rho_0 + \beta(c - c_0)\rho_0, \quad (1)$$

where the constant  $\rho_0 \geq 0$  is the initial water density and  $\beta \geq 0$  is the expansion coefficient of dissolved  $\text{CO}_2$  in groundwater. We work with scaled concentration  $c^* \in [0, 1]$ , given by

$$c = (c_D - c_0)c^* + c_0. \quad (2)$$

To formulate the governing equations in non-dimensional form, we denote dimensionless

variables by the superscript ‘ $\star$ ’ and we introduce:

$$\mathbf{u} = \frac{\kappa\beta(c_D - c_0)\rho_0 g}{\mu} \mathbf{u}^\star, \quad (3)$$

$$p = \beta(c_D - c_0)\rho_0 g H p^\star, \quad (4)$$

$$t = \frac{H\mu}{\kappa\beta(c_D - c_0)\rho_0 g} t^\star, \quad (5)$$

$$\mathbf{x} = H \mathbf{x}^\star, \quad (6)$$

where  $\mathbf{u}$  is the Darcy velocity, the constants  $\kappa \geq 0$  and  $\mu > 0$  are the permeability and viscosity, respectively,  $g$  is the gravitational acceleration,  $p$  is the pressure field,  $H$  is the characteristic height of the domain,  $t$  is time and  $\mathbf{x}$  is spatial position.

We denote our domain of interest by  $\Omega \subset \mathbb{R}^2$ , with boundary  $\Gamma = \partial\Omega$  and outward unit normal vector to the boundary  $\mathbf{n}$ . The boundary is partitioned as depicted in Figure 1b. We formulate a time-dependent model, with time interval of interest denoted by  $I = [0, t_N)$ . We are interested in steady solutions, hence  $t_N$  will be chosen to be suitably large in numerical simulations. In terms of non-dimensional quantities, the continuity equation, the Darcy equation and the boundary conditions read:

$$\nabla^\star \cdot \mathbf{u}^\star = 0 \quad \text{on } \Omega \times I, \quad (7)$$

$$\mathbf{u}^\star = -\nabla^\star p^\star + c^\star \mathbf{e}_k \quad \text{on } \Omega \times I, \quad (8)$$

$$p^\star = p_D^\star \quad \text{on } \Gamma_c \times I, \quad (9)$$

$$\mathbf{u}^\star \cdot \mathbf{n} = 0 \quad \text{on } \Gamma_{\text{cap}} \times I, \quad (10)$$

$$\mathbf{u}^\star \cdot \mathbf{n} = -u_B^\star \quad \text{on } \Gamma_B \times I, \quad (11)$$

where  $\mathbf{e}_k$  is the unit vector in the direction in which gravity acts,  $p_D^\star$  is a prescribed pressure and  $u_B^\star \geq 0$  is the prescribed fluid velocity across the inflow boundary. The condition in (11) gives a background flow from right-to-left in Figure 1b.

The concentration of dissolved CO<sub>2</sub> is modelled by:

$$\frac{\partial c^\star}{\partial t^\star} + \nabla^\star c^\star \cdot \mathbf{u}^\star - \frac{1}{Ra} \nabla^\star \cdot \nabla^\star c^\star = 0 \quad \text{on } \Omega \times I, \quad (12)$$

$$c^\star \mathbf{u}^\star \cdot \mathbf{n} = \mathbf{u}^\star \cdot \mathbf{n} \quad \text{on } \Gamma_{c,\text{in}} \times I, \quad (13)$$

$$\frac{1}{Ra} \nabla^\star c^\star \cdot \mathbf{n} = 0 \quad \text{on } \Gamma_c \times I, \quad (14)$$

$$\left(-\frac{1}{Ra} \nabla^\star c^\star + c^\star \mathbf{u}^\star\right) \cdot \mathbf{n} = 0 \quad \text{on } (\Gamma_{\text{cap}} \cup \Gamma_B) \times I, \quad (15)$$

$$c^\star(x, 0) = 0 \quad \text{on } \Omega, \quad (16)$$

where  $\Gamma_{c,\text{in}}$  is the portion of  $\Gamma_c$  on which  $\mathbf{u}^\star \cdot \mathbf{n} < 0$ , the constant  $Ra$  is a Rayleigh number,

$$Ra = \frac{\kappa\beta(c_D - c_0)\rho_0 g H}{\mu D}, \quad (17)$$

and  $D \geq 0$  is the pore-scale diffusivity. The boundary condition in (13) ensures that the advective flux of CO<sub>2</sub> at the CO<sub>2</sub> trap boundary ( $x = 0$ ) has dimensionless concentration unity on the inflow parts of the boundary, while it is not prescribed on the outflow parts of the boundary. In steady state, equations (12)–(15) require that:

$$\int_{\Gamma_c} c^\star \mathbf{u}^\star \cdot \mathbf{n} \, ds = 0 \quad (18)$$

We work from this point onward with the non-dimensional equations, hence we drop the ‘ $\star$ ’ superscript in the following.

### 3 Physical discussion

The above non-dimensionalisation identifies two controlling parameters:  $u_B$  represents the ratio of the background flow speed to the buoyancy-driven flow speed, and  $Ra$  represents the buoyancy-driven flow speed compared to the effective speed associated with vertical diffusive transport across the flow domain. These two parameters may be used to delineate the different flow regimes which may develop. We explore this below.

#### 3.1 Gravity intrusion model

In the case of weak diffusion, we expect that a nearly static intrusion of the dense  $\text{CO}_2$  saturated fluid extends upstream into the aquifer, and that this is balanced by the pressure gradient of the oncoming hydrostatic flow. There will be a thin diffusive boundary layer between the intrusion of  $\text{CO}_2$  saturated water and the oncoming flow of groundwater. If the intrusion extends far into the aquifer ( $X \gg 1$ ), then the continuity equation suggests that the background flow will be largely parallel to the boundary of the domain. To model this regime, we assume a sharp interface in the concentration field at a height  $h(x)$  above the lower boundary of the aquifer, where  $0 \leq h(x) \leq 1$ . This interface delineates the  $\text{CO}_2$  saturated intrusion and the overlying groundwater. Assuming the pressure in the intrusion is approximately hydrostatic (c.f. Huppert and Woods [5], Woods [16]), then in equilibrium the buoyancy driven pressure gradient in the  $x$ -direction along the intrusion matches the pressure gradient associated with the background flow above the intrusion, which has speed  $u_B/(1-h)$ . This leads to the balance

$$-(1-h)\frac{dh}{dx} = u_B. \quad (19)$$

The shape of the intrusion is therefore given by

$$h(x) = 1 - \sqrt{2u_B x}, \quad (20)$$

and it follows that the extent of the intrusion into the aquifer is  $X_{\text{int}} = 1/2u_B$ . This implies that if  $u_B$  is small, the intrusion extends far upstream into the aquifer, relative to the vertical extent of the aquifer, and the assumption that the flow is one-dimensional is valid.

The dimensionless time-of-travel of the oncoming flow past this intrusion is given by  $\tau_{\text{int}} = \int_{X_{\text{int}}}^0 (1/u) dx = 1/(3u_B^2)$ . For the interface to remain sharp, the time should be small relative to the diffusion time,  $\tau_{\text{diff}} = Ra$ . This requires that  $Ra \gg 1/(3u_B^2)$  which may be expressed in the form:

$$u_B^2 Ra \gg \frac{1}{3}. \quad (21)$$

For simplicity, we will henceforth use the condition  $u_B^2 Ra \gg 1$ .

When  $u_B$  is large, we expect any intrusion will become progressively smaller, with  $X_{\text{int}} \leq 1/u_B$  (for example Figure 9a, Section 4.2) and so we now expect the time-scale  $1/u_B^2$  to be an upper bound on the advection time,  $\sim X_{\text{int}}/u_B$ . Since  $X_{\text{int}} < 1$  for large  $u_B$ , we compare this with the diffusion time along, rather than across, the aquifer. This diffusion time scales as  $X_{\text{int}}^2 Ra$  and suggests that the line  $Ra = 1$  provides an upper bound on the transition from the diffusion to the advection regime. We return to this case in Section 4.2.

#### 3.2 Buoyancy-driven shear dispersion model

In the case  $u_B^2 Ra \ll 1$ , diffusion in the vertical direction will be relatively fast, hence the vertical gradient in concentration across the aquifer will be small. However, there may be a significant gradient in the along-aquifer direction. This can lead to different regimes in which diffusion is important and we now establish conditions which determine whether a buoyancy-driven shear flow develops or a simple advection–diffusion balance controls the transport. We explore these

two limits by starting from the full equations and allowing for variations in the concentration of CO<sub>2</sub> in the fluid associated with the diffusive flux. We follow largely the analysis of Szulczewski et al. [12] and Woods [16] to formulate a one-dimensional asymptotic model for the long-time evolution of the vertically averaged concentration field, but now in the presence of a background flow.

We decompose the CO<sub>2</sub> concentration of the groundwater in the form  $c(x, y, t) = \bar{c}(x, t) + \hat{c}(x, y, t)$ , where  $\bar{c}$  is the average concentration across the depth of the aquifer:

$$\bar{c} = \int_0^1 c \, dy. \quad (22)$$

Under the assumptions that the concentration fluctuations  $\hat{c}$  are small, as expected in the limit  $u_B^2 Ra \ll 1$ , and that the horizontal scale of the flow is much larger than the thickness of the aquifer, as expected in the case  $u_B \ll 1$ , the non-hydrostatic vertical pressure gradient is relatively small and the flow is approximately parallel to the boundaries of the flow domain. Therefore the pressure may be approximated by:

$$p = p_0 - y\bar{c}, \quad (23)$$

where  $p_0 = p_0(x, t)$  is the pressure at the base of the aquifer.

We decompose the velocity of the fluid  $\mathbf{u} = (u, v)$  into a sum of the average across the depth of the aquifer  $\bar{\mathbf{u}} = (\bar{u}, \bar{v})$  and the fluctuation  $\hat{\mathbf{u}} = (\hat{u}, \hat{v})$ , where:

$$\bar{\mathbf{u}} = \int_0^1 \mathbf{u} \, dy. \quad (24)$$

Using the approximation for the pressure (23), Darcy's law implies that

$$u = -\frac{\partial p_0}{\partial x} + y\frac{\partial \bar{c}}{\partial x}, \quad (25)$$

and so

$$\hat{u} = \frac{\partial \bar{c}}{\partial x} \left( y - \frac{1}{2} \right). \quad (26)$$

Taking the vertical average of the transport equation (12), and combining with the continuity equation (7), it may be shown that

$$\frac{\partial \bar{c}}{\partial t} + \bar{u} \frac{\partial \bar{c}}{\partial x} + \overline{\hat{u} \frac{\partial \bar{c}}{\partial x}} + \frac{\partial \overline{\hat{u} \bar{c}}}{\partial x} = \frac{1}{Ra} \frac{\partial^2 \bar{c}}{\partial x^2}. \quad (27)$$

Subtracting (27) from the transport equation, we obtain an equation governing the evolution of the concentration fluctuation:

$$\frac{\partial \hat{c}}{\partial t} + \hat{u} \frac{\partial \bar{c}}{\partial x} + \bar{u} \frac{\partial \hat{c}}{\partial x} + \hat{u} \frac{\partial \hat{c}}{\partial x} + \hat{v} \frac{\partial \hat{c}}{\partial y} = \frac{1}{Ra} \left( \frac{\partial^2 \hat{c}}{\partial x^2} + \frac{\partial^2 \hat{c}}{\partial y^2} \right) + \overline{\hat{u} \frac{\partial \hat{c}}{\partial x}} + \frac{\partial \overline{\hat{u} \hat{c}}}{\partial x}. \quad (28)$$

After long time periods, we expect the dominant balance in equation (28) to be between the distortion of the mean concentration due to the shear flow and the cross layer diffusion [13]. This gives rise to the following dominant balance, which can be shown *a posteriori*:

$$\frac{1}{Ra} \frac{\partial^2 \hat{c}}{\partial y^2} = \hat{u} \frac{\partial \bar{c}}{\partial x}. \quad (29)$$

Inserting (26) into (29) and integrating leads to the expression

$$\hat{c} = Ra \left( \frac{\partial \bar{c}}{\partial x} \right)^2 \left( \frac{y^3}{6} - \frac{y^2}{4} + \frac{1}{24} \right). \quad (30)$$

Combining this expression with the expression for  $\hat{u}$  in (26), the depth-averaged transport equation (27) becomes:

$$\frac{\partial \bar{c}}{\partial t} - u_B \frac{\partial \bar{c}}{\partial x} = \frac{1}{Ra} \frac{\partial^2 \bar{c}}{\partial x^2} + \frac{Ra}{120} \frac{\partial}{\partial x} \left( \frac{\partial \bar{c}}{\partial x} \right)^3. \quad (31)$$

At long times, (31) admits steady solutions in which  $\bar{c} \rightarrow 0$  as  $x \rightarrow \infty$ . In the limit that  $u_B^2 Ra \ll 1$ , the vertical gradient of concentration is small, and so in this limit it follows from the boundary condition in (13) that these solutions also require  $\bar{c} \approx 1$  at  $x = 0$ . To help interpret these solutions, it is convenient to re-scale the horizontal coordinate according to

$$x = \left( \frac{Ra}{120u_B} \right)^{\frac{1}{3}} \tilde{x}, \quad (32)$$

leading to the relation

$$-\frac{\partial \bar{c}}{\partial \tilde{x}} = \alpha \frac{\partial^2 \bar{c}}{\partial \tilde{x}^2} + \frac{\partial}{\partial \tilde{x}} \left( \frac{\partial \bar{c}}{\partial \tilde{x}} \right)^3, \quad (33)$$

where

$$\alpha = \left( \frac{120}{Ra^4 u_B^2} \right)^{\frac{1}{3}}. \quad (34)$$

We see that for large  $\alpha$  diffusion dominates ( $-\bar{c} = \alpha \bar{c}'$ ), and for small  $\alpha$  dispersion is dominant ( $-\bar{c} = \bar{c}'^3$ ). We have not found an analytic solution to (33), but in the two limits  $\alpha \gg 1$  and  $\alpha \ll 1$  there are useful analytical approximations.

In the limit  $\alpha \ll 1$ , the buoyancy-driven dispersion balances the advection. The solution to (33) when  $\alpha = 0$  is:

$$\bar{c} = \left( 1 - \frac{2}{3} \left( \frac{120u_B}{Ra} \right)^{\frac{1}{3}} x \right)^{\frac{3}{2}}. \quad (35)$$

Substitution of this solution into equation (28) and comparison of terms identifies that the dominant balance is indeed given by (29), in the limit  $u_B^2 Ra \ll 1$  and  $u_B < 1$ . The flow extends a large distance upstream compared to the thickness of the aquifer and the cross-flow diffusion is fast compared to the time for the background flow to pass through the region in which there is an elevated CO<sub>2</sub> concentration. The solution (35) suggests that the region of enhanced concentration advances upstream a non-dimensional distance

$$X_{\text{dis}} = \frac{3}{2} \left( \frac{Ra}{120u_B} \right)^{\frac{1}{3}}. \quad (36)$$

In the limit  $\alpha \gg 1$  the steady-state is dominated by a balance of advection and diffusion, and the solution may be approximated by

$$\bar{c} = e^{-Ra u_B x}, \quad (37)$$

with a characteristic length scale of

$$X_{\text{diff}} = -\frac{\ln c_{\text{diff}}}{Ra u_B}, \quad (38)$$

where  $c_{\text{diff}}$  is the concentration at which we consider it to be negligible.

Equating  $X_{\text{diff}}$  and  $X_{\text{dis}}$ , we find that

$$\alpha_e = \frac{3}{2 \ln c_{\text{diff}}}, \quad (39)$$

and this provides an indication of the transition between diffusive and dispersive mechanisms. For  $c_{\text{diff}} = 0.01$ , we find  $\alpha_e = 0.326$ . Figure 2 shows  $X_{\text{dis}}$  and  $X_{\text{diff}}$  as function of  $Ra$  for two different values of the background flow, using  $c_{\text{diff}} = 0.01$ . For larger Rayleigh numbers, dispersion controls the distance that the CO<sub>2</sub> front extends upstream.

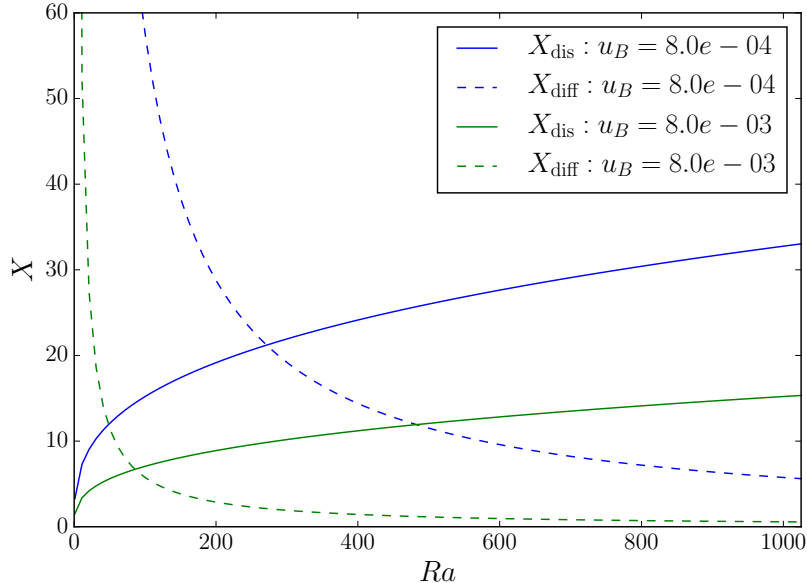


Figure 2: The distance the CO<sub>2</sub> front extends upstream in the dispersion limit and in the diffusion limit as a function of  $Ra$  for two different values of background flow  $u_B$ . Distances  $X$  correspond to multiples of the aquifer height  $H$ .

### 3.3 Regime differentiation

Combining the analysis of the gravity intrusion with the model of the buoyancy-driven shear dispersion, we infer that for  $u_B < O(1)$  three regimes may arise, as shown in Figure 3. Gravity intrusion occurs when  $u_B^2 Ra \gg 1$ . When  $u_B^2 Ra \ll 1$ , either a diffusion or dispersion dominated flow results, depending on the parameter  $\alpha$  (see equation (34)).

As  $u_B$  approaches unity, the above analysis shows that the transition between the dispersion and diffusion regimes and between the dispersion and intrusion regimes converge. In the case  $u_B \geq O(1)$ , the flow becomes more restricted in lateral extent upstream of the anticline, and our analysis of time-scales for  $u_B > 1$  given at the end of Section 3.1, suggests that with  $u_B > O(1)$ , an upper bound for the case in which the along-aquifer diffusion dominates the intrusion regime is  $Ra = 0(1)$ . In the diffusion dominated regime, from the boundary conditions (13) and (14), we expect that at  $x = 0$ ,  $\bar{c} < 1$  and we explore this further in Section 4.2 below. In Figure 3, we illustrate this upper bound with a dotted line, which for convenience we show as  $Ra = 4.93$  so that it intersects the point at which the solid and dashed lines converge.

## 4 Comparison of analytical and numerical models

To support the asymptotic analysis, the full problem in Section 2 has been solved on a domain of length  $L = 100$  and height  $H = 1$ . We use a mixed finite element method for the Darcy flow, and an upwinded discontinuous Galerkin method for the transport equation. Problems are advanced in time until a steady-state is reached. A detailed description of the numerical method and the complete computer code used to produce all examples is provided in the supporting material [14]. The computer code is built on the FEniCS libraries [8].

### 4.1 Weak background flows ( $u_B < 1$ )

To illustrate the form of the velocity and concentration fields for the three different regimes when  $u_B < 1$ , we show in Figure 4 the computed concentration field for three different values of



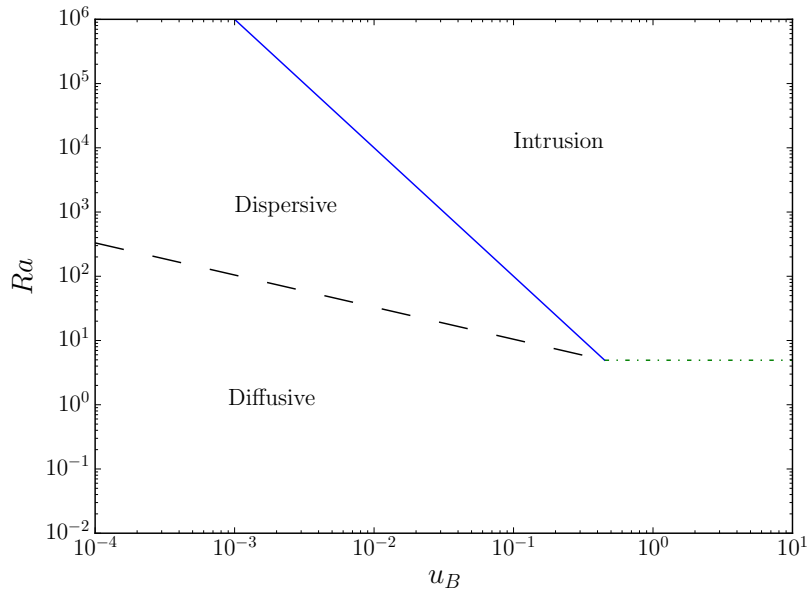


Figure 3: Illustration of the different regimes. The dashed line denotes  $\alpha = 1$  (see equation (34)) which delineates the dispersive and diffusive regimes for  $u_B < O(1)$ . The solid line shows  $Ra = 1/u_B^2$  (see equation (21)) and delineates the boundary between the intrusion regime and (i) the dispersive regime for  $u_B < O(1)$  and (ii) the diffusive regime for  $u_B > O(1)$ . The dotted line  $Ra = 4.93$  denotes an upper bound on the transition between the intrusive and diffusive regimes in the case  $u_B > 1$ , when the intrusion is relatively short, and the along-aquifer diffusive transport dominates the cross-aquifer diffusion; we have chosen  $Ra = 4.93$ , so that this line intersects the point where the dashed and solid lines converge.

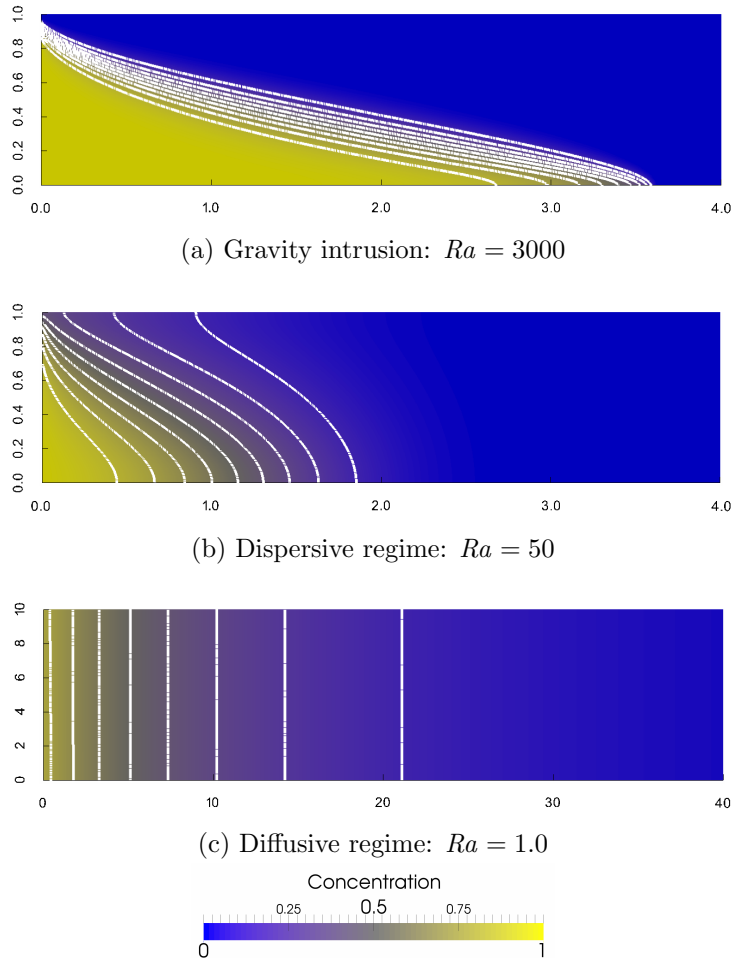


Figure 4: Concentration contours for  $u_B = 0.1$  and different values of  $Ra$ . The colours show the concentration locally as defined by the scale in the figure and the contour lines are shown at equal intervals of 0.1 from 0.1 to 0.9. The  $x$ -axis is longer in (c) than (a) or (b) to display the full diffusive regime.

$Ra$  when  $u_B = 0.1$ . The values of  $Ra$  correspond to points in the gravity intrusion, dispersion dominated, and diffusion dominated regimes.

#### 4.1.1 Concentration profiles

Figure 5 shows the vertically averaged concentration as a function of position along the aquifer for the one-dimensional model as given by (33) (dashed lines) and the two-dimensional full numerical calculations (solid lines) for  $u_B = 8 \times 10^{-4}$  and values of  $Ra$  ranging from 100 to 10000. The one-dimensional model (equation (33)) was solved using the FEniCS libraries and the full code is included in the supporting material [14]. There is very good agreement between the two models when  $Ra \leq 1000$  and the flow is in either the dispersion or diffusion dominated regime. The limiting dispersive (35) and diffusive (37) cases (heavy black lines as shown in legend) are also shown in the figure, and coincide with the two-dimensional numerical simulation when in the appropriate limit regimes.

When  $Ra = 10000$ , the problem is entering the gravity intrusion regime. In Figure 5 the two-dimensional numerical solution for this case no longer matches the one-dimensional dispersion dominated model in (33) since there are significant fluctuations in concentration across the height of the aquifer. In this regime the solution has a narrow vertical region of adjustment in

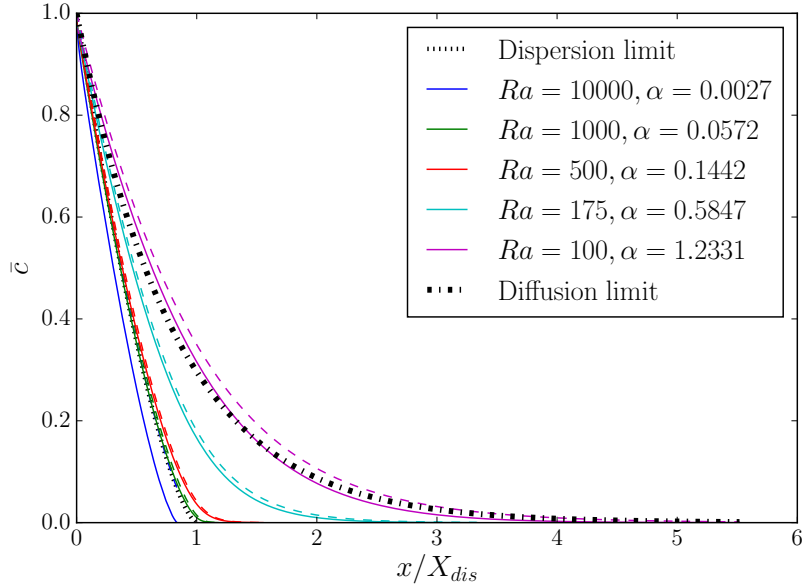


Figure 5: Computed and analytical variation of  $\bar{c}$  with  $x$  for different values of  $Ra$  when  $u_B = 8 \times 10^{-4}$ . The solid lines represents the two-dimensional numerical solution and the dashed lines represent the one-dimensional solution.

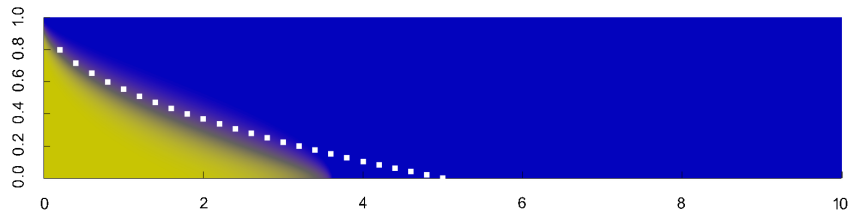


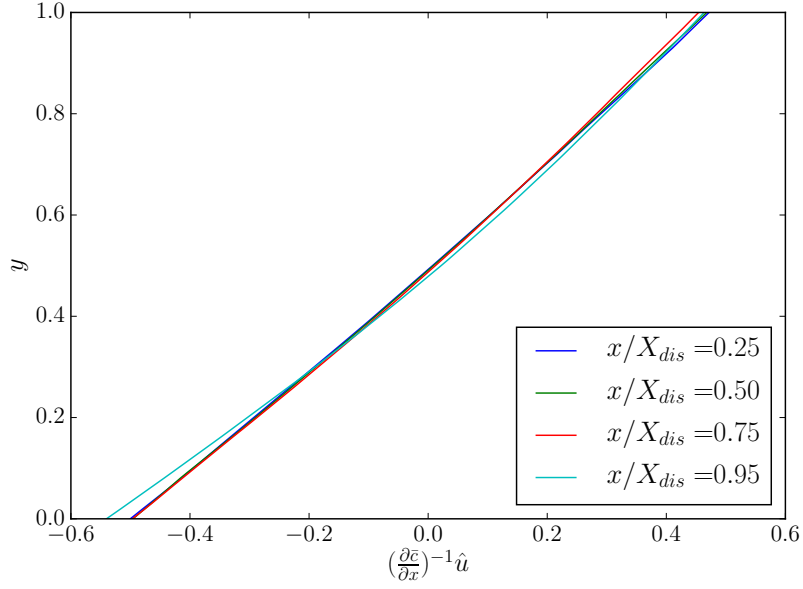
Figure 6: Concentration as a function of position for the gravity intrusion case with  $u_B = 0.1$  and  $Ra = 3000$  and the prediction of the intrusion model (equation 20) for the interface position overlaid (dotted line).

the concentration field from the  $\text{CO}_2$  saturated fluid at the base of the aquifer to the unsaturated oncoming groundwater at the top of the aquifer, reminiscent of the intrusion model given in Section 3.1.

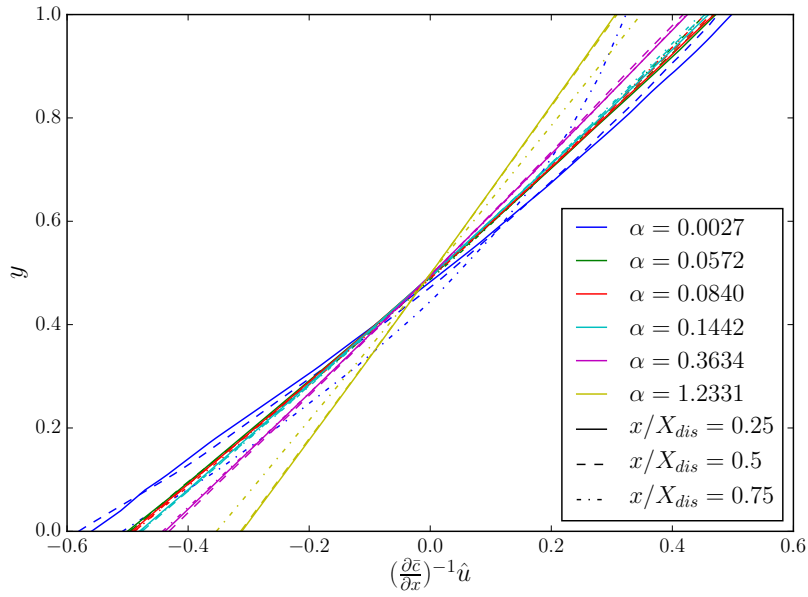
Indeed, in Figure 6 we compare the numerical solution for the concentration in the case  $Ra = 3000$  and  $u_B = 0.1$  with the prediction of the interface height  $h$  as predicted by equation (20) for the gravity intrusion model. That model treats the adjustment of the concentration from the  $\text{CO}_2$  saturated fluid to the oncoming groundwater flow, as a sharp interface. There is a reasonable match for  $x < 3.5$ . However, the diffusive boundary layer which is present in the full numerical solution leads to a weak recirculation that is not included in the intrusion model.

#### 4.1.2 Velocity fluctuation profiles

In the buoyancy driven dispersion regime, which arises for small  $\alpha$  and when  $u_B^2 Ra \ll 1$ , equation (26) predicts that the velocity variation from the mean flow  $\hat{u}$  will vary linearly with depth. If  $\hat{u}$  is divided by the depth-averaged concentration gradient, the profiles are predicted to pass through  $-0.5$  at  $y = 0$  and  $0.5$  at  $y = 1$ . Figure 7a shows the scaled velocity profiles computed from the two-dimensional model for  $Ra = 1000$  and  $u_B = 8 \times 10^{-4}$  ( $\alpha = 0.0527$ ). For  $x \lesssim (3/4)X_{dis}$  the velocity profiles are linear, whereas close to the stall point ( $x/X_{dis} = 1$ ) the profile begins to deviate from the simplified theory.



(a) Velocity fluctuations  $\hat{u}$  scaled by concentration gradient for  $Ra = 1000$  and  $u_B = 8 \times 10^{-4}$  ( $\alpha = 0.0527$ ).



(b) Velocity fluctuations  $\hat{u}$  for different values of  $\alpha$  at different values of  $x$ .

Figure 7: Scaled velocity profiles at different points along the domain for different values of  $\alpha$  with  $u_B = 8 \times 10^{-4}$ .

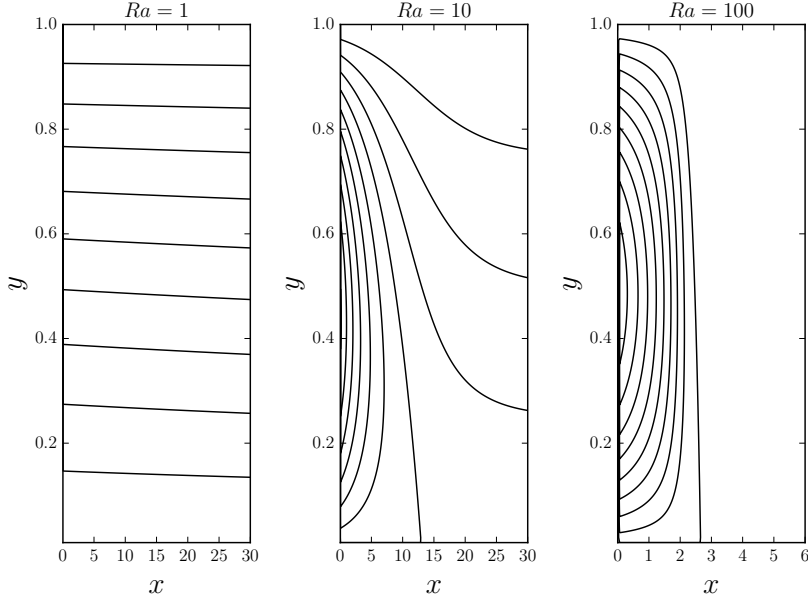


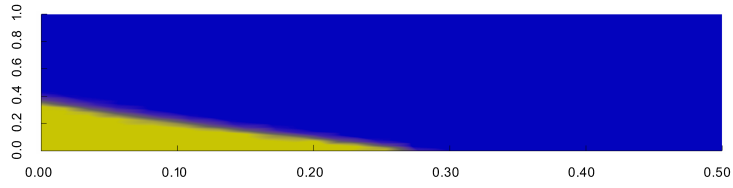
Figure 8: Typical streamlines of the flow for  $u_B = 0.01$  and  $Ra = 1, 10$  and  $100$ .

When in the regime where diffusion is important ( $u_B^2 Ra \ll 1$ ), as  $\alpha$  increases and the flow transitions from dispersive to diffusive, the one-dimensional analytical model becomes less applicable for  $\hat{u}$ . This can be seen in Figure 7b, where the scaled horizontal velocity fluctuations are shown at different distances into the domain for different values of  $\alpha$ . For  $0.0572 \leq \alpha \leq 0.1442$ , the scaled horizontal velocity fluctuations at different distances into the domain all lie on a straight line between  $-0.5$  and  $0.5$ . As  $\alpha$  increases, the numerically computed profiles deviate from the model, as the lateral diffusive transport becomes comparable to and then progressively more significant than the shear dispersion, but in this diffusion limit these perturbation velocities are very small compared to the background hydrological flow. When  $Ra = 10000$  and  $u_B = 8 \times 10^{-4}$  ( $\alpha = 0.0027$ ) the gravity intrusion region is being approached and the vertical concentration fluctuations across the domain are no longer small and so the velocity fluctuations are no longer governed by equation (26).

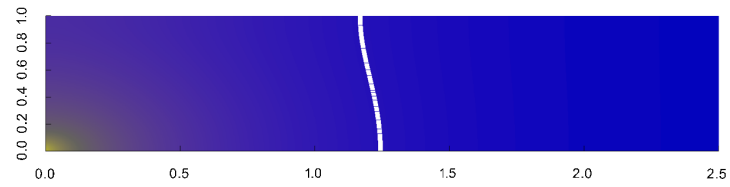
In Figure 8, we present a picture of the typical streamlines for the flow when  $u_B = 0.01$  and  $Ra = 1, 10$  and  $100$ . The streamlines are computed, approximately, by solving equation (33) numerically and inserting the result into (26), and then adding on the background hydrological flow. The case  $Ra = 1$  corresponds to the diffusion limit, the case  $Ra = 100$  corresponds to the dispersion regime, and the case  $Ra = 10$  is an intermediate case. The figure shows that in the diffusion limit the oncoming groundwater flow is dominant and the flow remains nearly uniform, but as  $Ra$  increases, some fluid begins to flow upstream leading to a small circulation in the lower part of the aquifer. As  $Ra$  increases further, and the flow is controlled by the buoyancy driven dispersion, a strong recirculation develops upstream of the anticline, leading to the diversion of the oncoming groundwater flow towards the top of the aquifer.

## 4.2 Strong background flows ( $u_B \gtrsim 1$ )

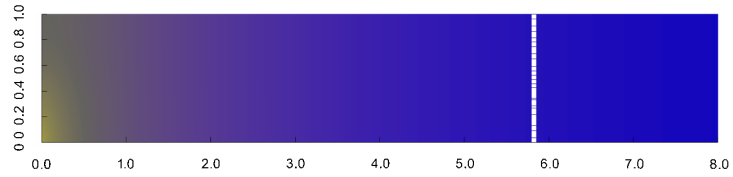
We now look at the case with a stronger background flow ( $u_B \gtrsim 1$ ). Three examples of full numerical solutions are shown in Figure 9 corresponding to  $Ra = 1000, 2$  and  $0.5$  for  $u_B = 1.0$ . In contrast to the case  $u_B < O(1)$ , only two distinct regimes develop (figure 3). Now, the flow transitions from the gravity intrusion regime to the diffusion dominated adjustment of the concentration since, with large  $u_B$ , the upstream extent of the buoyancy driven flow is insufficient for the buoyancy driven dispersion to develop before the along aquifer diffusion



(a) Gravity intrusion regime:  $Ra = 1000$



(b) Transitional regime:  $Ra = 2$



(c) Diffusive regime:  $Ra = 0.5$

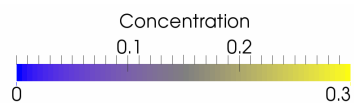


Figure 9: Concentration fields for different values of  $Ra$  for  $u_B = 1.0$ . The white contour in (b) and (c) is the  $c = 0.01$  contour. The presented domains have been truncated at different lengths to best show each regime. Note that the maximum concentration for the colour bar is set equal to 0.3, which is greater than the highest concentration for panels (b) and (c).

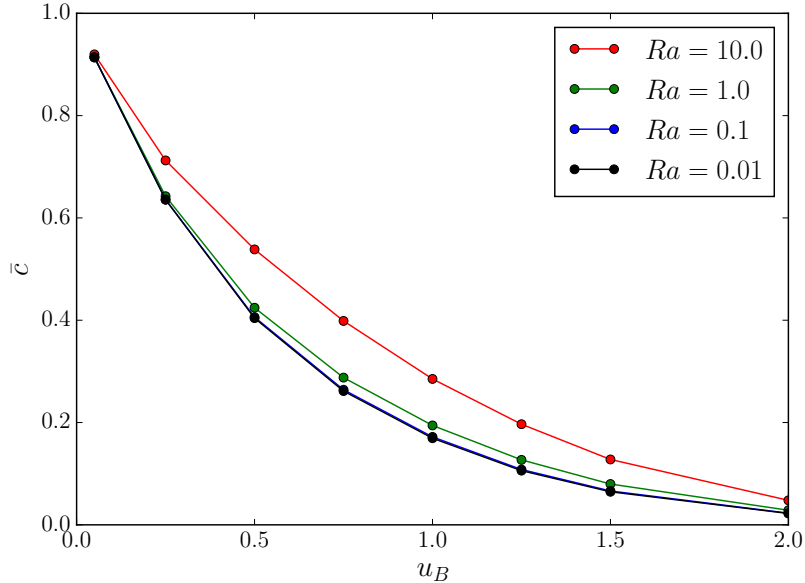


Figure 10: Computed vertically averaged concentration for various values of  $Ra$  and  $u_B$  at  $x = 0$ .

becomes significant. With large  $Ra$ , the solution is similar to the gravity-driven intrusion solution (Figure 9a), while for smaller values of  $Ra$  the solution evolves towards the along aquifer diffusion solution (Figure 9c).

We have calculated the vertically averaged mean concentration at  $x = 0$  from the numerical solutions for the cases when  $Ra = 10, 1, 0.1$  and  $0.01$ , as shown in Figure 10. As  $u_B$  increases,  $\bar{c}$  decreases at  $x = 0$  since there is a progressively stronger flow from the upstream region which suppresses the upstream buoyancy driven flow of dense,  $\text{CO}_2$  saturated fluid from below the anticline

In the diffusive regime, which we expect to apply for small  $Ra$ , the vertically averaged concentration may be approximated by the diffusive solution of equation (33), given by:

$$\bar{c}(x) = \bar{c}(0)e^{-Ra u_B x}. \quad (40)$$

Figure 11 shows the vertically-averaged concentration profiles for the three values of  $Ra$  and  $u_B = 1.0$ . Using the numerically determined value for the mean concentration at  $x = 0$ , we have compared the vertically averaged concentration with the diffusion solution given by equation (40). When  $Ra = 0.1$ , the system is in the diffusion regime and the numerical solution for  $\bar{c}$  matches the diffusion profile. When  $Ra \geq 1$ , the simulations move towards the intrusion regime and the numerical solutions evolve away from the approximate analytical solution.

## 5 Conclusions

We have explored both analytically and numerically the long-term dissolution of a plume of  $\text{CO}_2$  trapped in an anticline and driven by a steady background flow of  $\text{CO}_2$  unsaturated water from upstream. We have focused on the role of diffusion and buoyancy-driven flow in regulating the distribution of  $\text{CO}_2$  in the aquifer fluid upstream of the anticline. In the case  $u_B < 1$ , where  $u_B$  is the dimensionless background hydrological flow, the buoyancy-driven speed of the dense  $\text{CO}_2$  saturated water exceeds the oncoming flow speed and the  $\text{CO}_2$  extends a significant distance upstream of the anticline ( $x \gg H$ ). In this case, we have established that three different regimes may develop. With a small diffusive flux across the aquifer ( $u_B^2 Ra \gg 1$ , where  $Ra$  is the Rayleigh number associated with the dense  $\text{CO}_2$  laden fluid), a static intrusion of dense

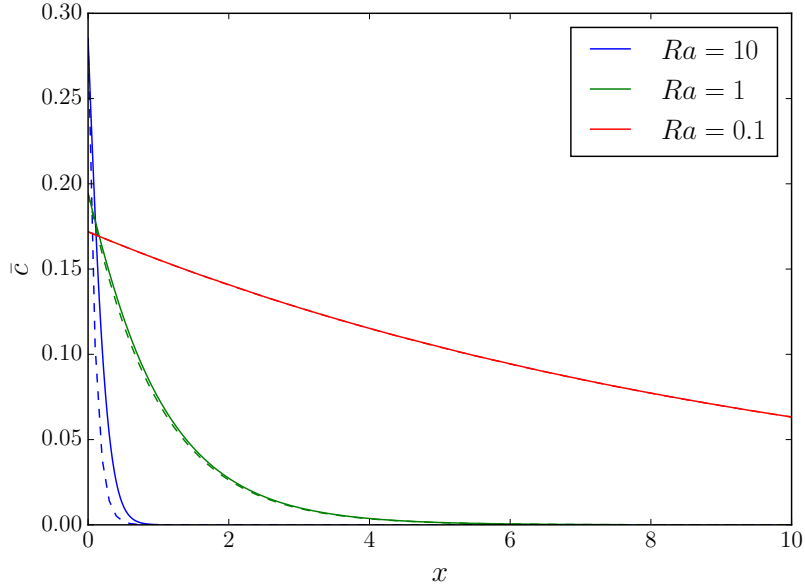


Figure 11: Computed and analytical variation of  $\bar{c}$  with  $x$  for different values of  $Ra$  when  $u_B = 1.0$ . The solid line represents the two-dimensional numerical solution and the dashed line represents the diffusion limit if using the numerically computed  $\bar{c}$  as the boundary condition at  $x = 0$ .

$\text{CO}_2$  saturated fluid develops and extends a distance  $1/2u_B$  upstream of the anticline. This is balanced by the pressure gradient in the oncoming flow. With larger diffusive fluxes across the aquifer ( $u_B^2 Ra \ll 1$ ) we have established that a buoyancy-driven shear dispersion flow regime may develop and a convective recirculation develops just upstream of the aquifer, regulated by (i) the supply of unsaturated aquifer fluid from upstream; (ii) the buoyancy-driven flow associated with the dense  $\text{CO}_2$  saturated fluid from downstream; and (iii) the vertical diffusion of  $\text{CO}_2$  across the aquifer. However, if the diffusive transport is too rapid ( $\alpha \ll 1$ ) then a simple advection-diffusion balance regulates the distribution of the  $\text{CO}_2$  in solution in the water upstream of the anticline. In the case  $u_B > 1$ , the  $\text{CO}_2$  extends a much smaller distance upstream from the anticline, and in this case, either only the advection-diffusion balance or the intrusion regimes develop.

In the context of  $\text{CO}_2$  sequestration in deep saline aquifers, this analysis is important as it demonstrates the strong effect that a background hydrological flow has on the long-term dissolution of  $\text{CO}_2$  in a structural trap. We now show that under some typical conditions the dynamics may indeed be controlled by a balance between the buoyancy-driven shear dispersion and the background hydrological flow. This leads to new estimates of the maximum upstream migration of  $\text{CO}_2$  rich groundwater. The solubility of  $\text{CO}_2$  in groundwater is only a few wt%, so if we consider a plume of  $\text{CO}_2$  of order 10 m deep, trapped in a structural anticline and connected to a laterally extensive aquifer of order 20–30 m deep, then vertical convective dissolution alone will only lead to dissolution of order 0.2–0.6 m. Continued dissolution will require the lateral supply of undersaturated water from the aquifer and this may be achieved through a combination of buoyancy-driven lateral dispersion of the dense  $\text{CO}_2$  saturated water from below the  $\text{CO}_2$  plume and supply of water resulting from a background hydrological flow. For typical conditions, with permeability of order 0.1–0.01 Darcy, a density difference of order a few percent between the undersaturated and saturated water, and an aquifer diffusivity of order  $10^{-9}$ – $10^{-10}$   $\text{m}^2/\text{s}$ , the Rayleigh number will be of order  $10^3$ – $10^4$ . With a hydrological flow speed of order  $10^{-8}$ – $10^{-9}$   $\text{m/s}$ , the dimensionless velocity  $u_B$  will be of order 0.01–1.0. From Figure 3 we see that it is the transport associated with the shear dispersion that balances the steady background flow. We estimate that the length scale of the dispersive transport (equation (36)) will be of order



100–400 m. Once the steady flow regime is established, the continued dissolution will occur at a rate proportional to the supply of undersaturated water in the hydrological flow, as given in non-dimensional form by  $u_B(c_D - c_0)$ . For an anticline whose extent in the direction of the flow is of order 1000 m, and with a CO<sub>2</sub> plume with initial depth of order 10 m, then in order to dissolve, this will require a net flow of groundwater of order  $10^6$  m<sup>2</sup>, which will require a time of order  $10^{12}$ – $10^{13}$  s corresponding to  $10^5$ – $10^6$  years.

## Acknowledgements

HJTU was funded by an EPSRC Doctoral Training Partnership scheme (grant EP/J500380/1). Data relating to this publication is available in Unwin and Wells [14].

## References

- [1] J. Bear. *Dynamics of fluids in porous media*. Courier Corporation, 1972.
- [2] F. C. Boait, N. J. White, M. J. Bickle, R. A. Chadwick, J. A. Neufeld, and H. E. Huppert. Spatial and temporal evolution of injected CO<sub>2</sub> at the Sleipner Field, North Sea. *Journal of Geophysical Research: Solid Earth*, 117(B3), 2012. doi: 10.1029/2011JB008603. URL <http://dx.doi.org/10.1029/2011JB008603>. B03309.
- [3] M. A. Hesse, H. A. Tchelepi, B. J. Cantwel, and F. M. Orr. Gravity currents in horizontal porous layers: transition from early to late self-similarity. *Journal of Fluid Mechanics*, 577:363–383, 4 2007. ISSN 1469-7645. doi: 10.1017/S0022112007004685. URL [http://journals.cambridge.org/article\\_S0022112007004685](http://journals.cambridge.org/article_S0022112007004685).
- [4] D. R. Hewitt, J. A. Neufeld, and J. R. Lister. High rayleigh number convection in a three-dimensional porous medium. *Journal of Fluid Mechanics*, 748:879–895, 6 2014. ISSN 1469-7645. doi: 10.1017/jfm.2014.216. URL [http://journals.cambridge.org/article\\_S002211201400216X](http://journals.cambridge.org/article_S002211201400216X).
- [5] H. E. Huppert and A. W. Woods. Gravity-driven flows in porous layers. *Journal of Fluid Mechanics*, 292:55–69, 6 1995. ISSN 1469-7645. doi: 10.1017/S0022112095001431. URL [http://journals.cambridge.org/article\\_S0022112095001431](http://journals.cambridge.org/article_S0022112095001431).
- [6] IPCC. *Carbon dioxide capture and storage*. IPCC Geneva, Switzerland, 2005. URL [https://www.ipcc.ch/publications\\_and\\_data/\\_reports\\_carbon\\_dioxide.htm](https://www.ipcc.ch/publications_and_data/_reports_carbon_dioxide.htm). [https://www.ipcc.ch/publications\\_and\\_data/\\_reports\\_carbon\\_dioxide.htm](https://www.ipcc.ch/publications_and_data/_reports_carbon_dioxide.htm).
- [7] E. Lindeberg and D. Wessel-Berg. Vertical convection in an aquifer column under a gas cap of CO<sub>2</sub>. *Energy Conversion and Management*, 38:S229–S234, 1997. ISSN 0196-8904. doi: [http://dx.doi.org/10.1016/S0196-8904\(96\)00274-9](http://dx.doi.org/10.1016/S0196-8904(96)00274-9). URL <http://www.sciencedirect.com/science/article/pii/S0196890496002749>. Proceedings of the Third International Conference on Carbon Dioxide Removal.
- [8] A. Logg, K.-A. Mardal, and G. N. Wells, editors. *Automated Solution of Differential Equations by the Finite Element Method*, volume 84 of *Lecture Notes in Computational Science and Engineering*. Springer, 2012. doi: 10.1007/978-3-642-23099-8. URL <http://dx.doi.org/10.1007/978-3-642-23099-8>.
- [9] G. S. H. Pau, J. B. Bell, K. Pruess, A. A. S., L. M. J., and K. Zhang. Numerical studies of density-driven flow in CO<sub>2</sub> storage in saline aquifers. In *TOUGH Symposium 2009*, September 2009.

- [10] K. Pruess, T. Xu, J. Apps, and J. Garcia. Numerical modeling of aquifer disposal of CO<sub>2</sub>. *Society of Petroleum Engineers*, pages 49–60, 2003. doi: 10.2118/66537-MS. URL <https://www.onepetro.org/conference-paper/SPE-66537-MS>.
- [11] A. Riaz, M. Hesse, H. A. Tchelepi, and F. M. Orr. Onset of convection in a gravitationally unstable diffusive boundary layer in porous media. *Journal of Fluid Mechanics*, 548:87–111, 2 2006. ISSN 1469-7645. doi: 10.1017/S0022112005007494. URL [http://journals.cambridge.org/article\\_S0022112005007494](http://journals.cambridge.org/article_S0022112005007494).
- [12] M. L. Szulczewski, M. A. Hesse, and R. Juanes. Carbon dioxide dissolution in structural and stratigraphic traps. *Journal of Fluid Mechanics*, 736:287–315, 2013.
- [13] G. Taylor. Dispersion of soluble matter in solvent flowing slowly through a tube. *Proceedings of the Royal Society of London A: Mathematical, Physical and Engineering Sciences*, 219 (1137):186–203, 1953. ISSN 0080-4630. doi: 10.1098/rspa.1953.0139.
- [14] H. J. T. Unwin and G. N. Wells. Supporting material, 2015. URL <https://bitbucket.org/ettieunwin/co2-dissolution>. <https://bitbucket.org/ettieunwin/co2-dissolution>.
- [15] J. P. Verdon, J.-M. Kendall, A. L. Stork, R. A. Chadwick, D. J. White, and R. C. Bissell. Comparison of geomechanical deformation induced by megatonne-scale CO<sub>2</sub> storage at Sleipner, Weyburn, and In Salah. *Proceedings of the National Academy of Sciences*, 110 (30):E2762–E2771, 2013. doi: 10.1073/pnas.1302156110. URL <http://www.pnas.org/content/110/30/E2762.abstract>.
- [16] A. W. Woods. *Flow in Porous Rock*. Cambridge University Press, 2015.
- [17] A. W. Woods and T. Espie. Controls on the dissolution of CO<sub>2</sub> plumes in structural traps in deep saline aquifers. *Geophysical Research Letters*, 39(8), 2012. doi: 10.1029/2012GL051005. URL <http://dx.doi.org/10.1029/2012GL051005>. L08401.